Spin-orbital entanglement in d^8 Mott insulators: Possible excitonic magnetism in diamond lattice antiferromagnets

Fei-Ye Li and Gang Chen*

State Key Laboratory of Surface Physics and Department of Physics, Fudan University, Shanghai 200433, China
and Department of Physics and Center of Theoretical and Computational Physics, The University of Hong Kong, Hong Kong, China

(Received 5 September 2018; revised manuscript received 16 April 2019; published 3 July 2019)

Motivated by the recent activities on the diamond lattice antiferromagnet $NiRh_2O_4$ with Ni^{2+} $3d^8$ local moments, we theoretically explore on general grounds the unique spin and orbital physics for the diamond lattice antiferromagnet with $3d^8$ local moments. The superexchange interaction between the local moments usually favors magnetic orders. Due to the particular electron configuration of the $3d^8$ ion with a partially filled upper t_{2g} level and a fully filled lower e_g level, the atomic spin-orbit coupling becomes active at the linear order and would favor a spin-orbital-entangled singlet with quenched local moments in the single-ion limit. Thus, the spin-orbital entanglement competes with the superexchange and could drive the system to a quantum critical point that separates the spin-orbital singlet and the magnetic order. We further explore the effects of magnetic field and uniaxial pressure. The nontrivial response to the magnetic field is intimately tied to the underlying spin-orbital structure of the local moments. We discuss future experiments such as doping and pressure and point out the correspondence between different electron configurations.

DOI: 10.1103/PhysRevB.100.045103

I. INTRODUCTION

The spin-orbit coupling (SOC) is a relativistic effect and plays an important role in our understanding of the quantum-mechanical properties of quantum materials with heavy elements. Contrary to this conventional belief that explains the recent SOC activities in $4d/5d$ transition-metal compounds [1], SOC occasionally becomes important in $3d$ transition-metal materials, especially in the Mott insulating systems with orbital degeneracies [2]. It is well known that, in Mott insulators with pure spin moments, the atomic SOC enters via the high-order perturbation of the Hubbard model and generates the single-ion spin anisotropy and the Dzyaloshinskii-Moriya interaction [2]. Except in certain circumstances, these extra spin anisotropy and interactions can often be regarded as small perturbations to the (Heisenberg) exchange part of the interactions. When the system has an orbital degeneracy, however, the atomic SOC should be considered at the first place and would reconstruct local spin and orbital degrees of freedom. The diamond lattice antiferromagnet $FeSc_2S_4$ [3–12] with Fe^{2+} $3d^6$ local moments and various vanadates [2,13–15] provide physical realizations of such physics, where the former has an e_g orbital degeneracy, while the latter has a t_{2g} degeneracy.

In this paper, we study the diamond lattice antiferromagnet where the Ni^{2+} $3d^8$ ions are the magnetic ions. We are *partly motivated* by the experiments and the existence of the diamond lattice antiferromagnet $NiRh_2O_4$ [16], but we explore on general grounds the consequence of the atomic SOC of the Ni^{2+} ions. The compound $NiRh_2O_4$ is merely our motivation, and we explore the more general possibilities that may occur in principle. We point out that there exists keen competition between the atomic SOC at the single-ion level and the intersite superexchange interaction for a $3d$ transition-metal ion such as Ni^{2+}. The spin-orbital singlet would give way to the magnetically ordered state through a quantum phase transition when the superexchange interaction dominates over the atomic SOC. We further show the effect of the external magnetic field and the uniaxial pressure on the quantum criticality. The nontrivial structure of the phase diagram such as the re-entrant transition under the field directly reveals the underlying spin-orbital structure of the local moments. Although our motivation originates partly from the diamond lattice antiferromagnet $NiRh_2O_4$, the physics that we reveal in this paper may be easily extended to other magnets with similar crystal field schemes and orbital configurations. We further go beyond the specific case of the $3d^8$ ions, establish the *correspondence* between different electron configurations, and suggest the applicability to many other materials.

The rest of this paper is organized as follows. In Sec. II, we discuss the microscopics and propose our model for the $3d^8$ diamond lattice antiferromagnet. Combining the Weiss mean-field approach and the flavor-wave approach, we obtain the phase diagram of this model and discuss the criticality at the quantum phase transition in Sec. III. We then explore the effect of the external magnetic field and the uniaxial pressure in Secs. IV and V, respectively. Finally, in Sec. VI we summarize our results and discuss the potential relation of our theoretical results to experiments.

II. THE MICROSCOPICS AND OUR MODEL

We start with the microscopics of the Ni^{2+} $3d^8$ ion. In $NiRh_2O_4$, which initiated our motivation, the Ni^{2+} ion is in the tetrahedral crystal field environment, and as a result, the

*gangchen.physics@gmail.com

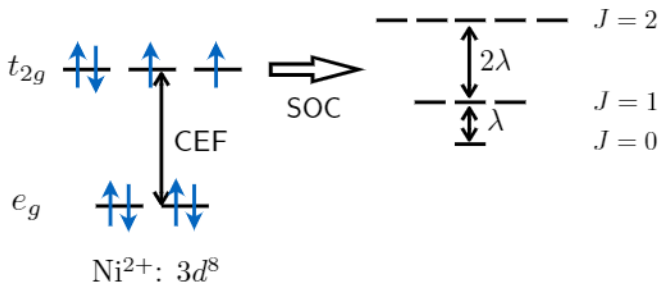

FIG. 1. The electron configuration of the $3d^8$ ion in the tetrahedral crystal field environment. When the atomic spin-orbit coupling (SOC) is introduced, the electron states in the upper t_{2g} levels are further split into the spin-orbital entangled J states. Here, "CEF" refers to the crystal electric field splitting.

t_{2g} levels are higher in energy than the e_g levels. As we show in Fig. 1 for the $3d^8$ electron configuration, the lower e_g levels are completely filled, and the t_{2g} levels are partially filled with four electrons. For our purposes here, we first ignore the further splitting within the t_{2g} manifold and include the specific physics in the later part of the paper. Because the t_{2g} levels are partially filled, the atomic SOC is active at the linear order. As the fully filled e_g manifold can be neglected, the local physics for the $3d^8$ electron configuration here is rather analogous to the one for the $4d^4/5d^4$ electron configurations of the Ru^{4+} or Ir^{5+} ions that were discussed in Refs. [17,18], where Ref. [18] proposed the interesting possibility of excitonic magnetism. For the t_{2g} manifold in Fig. 1, the local Hund's coupling first favors a total spin $S = 1$ local moment, and the remaining orbital occupation still has threefold degeneracy. The total orbital angular momentum remains unquenched and can be treated as an *effective* orbital angular moment $\boldsymbol{L}$ with $L = 1$ in the reduced Hilbert space of the three orbital occupations. The atomic SOC is then written as

$$H_{\text{soc}} = +\lambda \sum_i \boldsymbol{L}_i \cdot \boldsymbol{S}_i, \tag{1}$$

where the sign of the SOC is opposite to the case for two electrons in the t_{2g} manifold. The SOC here acts on the total spin and total orbital angular momentum of the four electrons and differs from the SOC at the single-electron level. The SOC entangles the spin and the orbitals and leads to a total moment J in the single-ion limit. The single-ion ground state is a spin-orbital singlet with $J = 0$, and the excited ones are $J = 1$ triplets and $J = 2$ quintuplets (see Fig. 1).

Besides the atomic SOC, the spin and orbital degrees of freedom on neighboring sites interact with each other through the superexchange interaction. Due to the orbital degeneracy, the exchange interaction should be of the Kugel-Khomskii form [19]. The superexchange path for both the first neighbor and second neighbor in the diamond lattice of spinel compounds involves five atoms [4,20]. Thus, the explicit derivation of the superexchange interaction is complicated and is not quantitatively reliable. Our purpose here is not to be quantitatively precise but to capture the generic physics of the competition between the spin-orbital entanglement and the tendency to magnetic ordering for the $3d^8$ diamond lattice antiferromagnet and the systems alike. Thus, we consider a simplified superexchange model with only spin interactions. The exchange model is given as

$$H_{\text{ex}} = \sum_{\langle ij \rangle} J_1 \boldsymbol{S}_i \cdot \boldsymbol{S}_j + \sum_{\langle\langle ij \rangle\rangle} J_2 \boldsymbol{S}_i \cdot \boldsymbol{S}_j, \tag{2}$$

where J_1 (J_2) is the first- (second-) neighbor exchange coupling. This simplified model captures the ordering tendency but is not supposed to capture the possibility of an (exotic) quantum spin-orbital liquid or quantum spin liquid with fractionalized excitations that was recently explored with the functional renormalization group calculation in Ref. [21] for the spin-1 diamond lattice antiferromagnet with frustrated spin interactions.

III. PHASE DIAGRAM AND QUANTUM CRITICALITY

Here, we study the full Hamiltonian that contains both SOC and the exchange interaction,

$$H = H_{\text{soc}} + H_{\text{ex}}. \tag{3}$$

Once our full model is written, the physics is almost transparent. In addition to the competition between SOC and exchange, the exchange frustration would further complicate our phase diagram. To establish the phase diagram, one approach is to start from the (nonmagnetic) spin-orbital singlet phase and study its magnetic instability to an ordered state by condensing the excitonic excitation. The resulting ordered state was dubbed the "excitonic magnetic state." This approach was used by Khaliullin for a more realistic exchange model on a square lattice [18] with $4d^4/5d^4$ ions such as Ca_2RuO_4 by truncating the physical Hilbert space to the $J = 0$ and $J = 1$ states, and the excitonic magnetism was introduced there. The other approach is to start from the ordered state and trace the fate of the magnetic order parameters as we increase the strength of the SOC. When the magnetic order disappears, the system enters the spin-orbital singlet phase. Both approaches are adopted in this work. Via a Weiss-type mean-field decoupling, our Hamiltonian becomes

$$H_{\text{MFT}} = H_{\text{soc}} + \sum_{\langle ij \rangle} J_1 \boldsymbol{S}_i \cdot \langle \boldsymbol{S}_j \rangle + \sum_{\langle\langle ij \rangle\rangle} J_2 \boldsymbol{S}_i \cdot \langle \boldsymbol{S}_j \rangle, \tag{4}$$

where $\langle \boldsymbol{S}_j \rangle$ is taken to be a mean-field order parameter. To choose a mean-field ansatz for the order parameter, we start from the limiting case with a vanishing SOC such that this limit has been well understood. Here, we consider the antiferromagnetic couplings $J_1 > 0$ and $J_2 > 0$. It was shown [20,22,23] that, for $J_2/J_1 < 1/8$, a Néel state with an order wave vector $\boldsymbol{q} = \boldsymbol{0}$ is obtained; for $J_2/J_1 > 1/8$, the ground state has a spiral configuration, and the degenerate order wave vectors form a spiral surface [20] in the momentum space and satisfy

$$\cos\frac{q_x}{2}\cos\frac{q_y}{2} + \cos\frac{q_x}{2}\cos\frac{q_z}{2} + \cos\frac{q_y}{2}\cos\frac{q_z}{2} = \frac{J_1^2}{16J_2^2} - 1. \tag{5}$$

When J_2/J_1 is increased from 1/8, this "spiral surface" emerges and surrounds $\boldsymbol{q} = \boldsymbol{0}$, showing a nearly spherical geometry. It then touches the boundary of the Brillouin zone at $J_2/J_1 = 1/4$ and develops "holes" on the boundary of

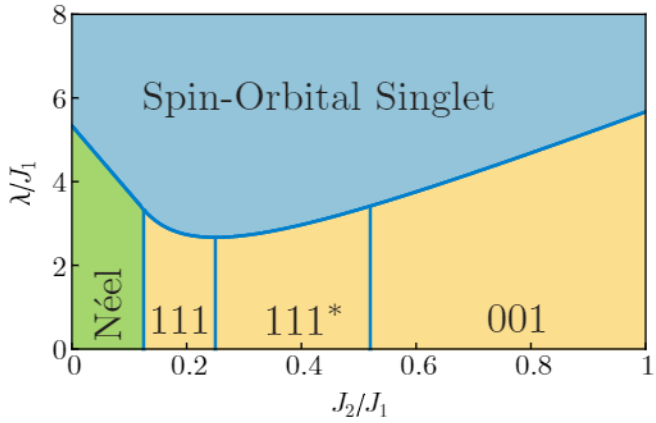

FIG. 2. The phase diagram of the full model in Eq. (3). This phase diagram summarizes the competition between the SOC and the superexchange interaction and captures the frustration of the exchange part. Refer to the main text for details about the magnetic orders.

the Brillouin zone, as J_2/J_1 is further increased. Finally, the spiral surface shrinks to lines corresponding to the degenerate ground-state manifold of two decoupled fcc lattices in the limit $J_2/J_1 \to \infty$. This degeneracy is lifted when quantum fluctuation is included, giving certain stabilized spiral orders [21,24,25]. For $1/8 < J_2/J_1 < 1/4$, the selected wave vectors are along the [111] direction. For $1/4 < J_2/J_1 \lesssim 1/2$, the [111] direction no longer intersects with the spiral surface, and the selected wave vectors are around the [111] direction. This region is labeled by [111*] in Fig. 2. When $J_2/J_1 \gtrsim 1/2$, quantum fluctuation favors the spiral orders with the wave vectors along the [001] direction.

From the known results, we set up a general mean-field ansatz as

$$\boldsymbol{r}_j \in \mathrm{I}, \quad \langle \boldsymbol{S}_j \rangle = \mathbb{M}\,\mathrm{Re}[(\hat{x} - i\hat{y})e^{i\boldsymbol{q}\cdot\boldsymbol{r}_j}], \tag{6}$$

$$\boldsymbol{r}_j \in \mathrm{II}, \quad \langle \boldsymbol{S}_j \rangle = \mathbb{M}\,\mathrm{Re}[(\hat{x} - i\hat{y})e^{i(\boldsymbol{q}\cdot\boldsymbol{r}_j + \phi_{\boldsymbol{q}})}], \tag{7}$$

where I and II refer to the two sublattices of the diamond lattice, $\boldsymbol{q}$ is the propagating wave vector of the spin spiral, and $\phi_{\boldsymbol{q}}$ is the phase shift between the two sublattices [20]. The order parameter $\mathbb{M}$ is determined self-consistently from the mean-field Hamiltonian H_{MFT}.

Our phase diagram is depicted in Fig. 2. When SOC is weak, the magnetic ordered phase is separated into the Néel order region and the spiral order regions (111, 111*, and 001). A transition from the magnetic ordered phase to the spin-orbital singlet occurs when increasing the strength of SOC. This transition is evidenced by the vanishing of $\mathbb{M}$ and is found to be continuous within our mean-field theory. The critical strength of SOC is $16(J_1/3 - J_2)$ for $J_2/J_1 < 1/8$ and $J_1^2/(3J_2) + 16J_2/3$ for $J_2/J_1 > 1/8$. As expected, when the frustration is large, a smaller critical SOC is needed to drive the transition. The smallest critical SOC is found at $J_2/J_1 = 1/4$.

To explore the critical properties, we start from the spin-orbital singlet and study its excitations and instability [18,26]. Removing the highly excited $J = 2$ quintuplets, we then rewrite our model using a representation with four flavors of bosons, $s_i, t_{ix}, t_{iy}, t_{iz}$, on each site i that are defined as

$$s_i^\dagger|0\rangle \equiv |0,0\rangle_i, \tag{8}$$

$$t_{ix}^\dagger|0\rangle \equiv i(|1,1\rangle_i - |1,-1\rangle_i)/\sqrt{2}, \tag{9}$$

$$t_{iy}^\dagger|0\rangle \equiv (|1,1\rangle_i + |1,-1\rangle_i)/\sqrt{2}, \tag{10}$$

$$t_{iz}^\dagger|0\rangle \equiv -i|1,0\rangle_i, \tag{11}$$

where the states are labeled $|J, J^z\rangle$ and $|0\rangle$ is the vacuum state. A local Hilbert space constraint,

$$s_i^\dagger s_i + \sum_\alpha t_{i\alpha}^\dagger t_{i\alpha} = 1, \tag{12}$$

is imposed with $\alpha = x, y, z$. In the spin-orbital singlet phase, the singlet boson s_i is condensed, with $\langle s_i \rangle \equiv s \neq 0$. With the above reformulation of the spin variables, we obtain a flavor-wave mean-field Hamiltonian for the triplet excitations,

$$H_{\mathrm{fMF}} = \sum_{ij,\alpha} \frac{J_{ij}}{3}(t_{i\alpha}^\dagger t_{j\alpha} + t_{i\alpha}^\dagger t_{j\alpha}^\dagger + \mathrm{H.c.}) + \lambda \sum_{i\alpha} t_{i\alpha}^\dagger t_{i\alpha}, \tag{13}$$

where the detailed derivation is given in Appendix A, and the triplon excitation is found as

$$\omega^\pm(\boldsymbol{q}) = \lambda^{\frac{1}{2}}(\lambda + 4J_{\boldsymbol{q}}^\pm/3)^{\frac{1}{2}}, \tag{14}$$

where

$$J_{\boldsymbol{q}}^\pm \equiv J_2 \sum_{\boldsymbol{b}_i} e^{i\boldsymbol{q}\cdot\boldsymbol{b}_i} \pm J_1 \left| \sum_{\boldsymbol{a}_i} e^{i\boldsymbol{q}\cdot\boldsymbol{a}_i} \right| \tag{15}$$

and $\{\boldsymbol{a}_i\}$ ($\{\boldsymbol{b}_i\}$) refer to the first- (second-) neighbor vectors. Both $\omega^\pm(\boldsymbol{q})$ are threefold degenerate, and the minimum of $\omega^-(\boldsymbol{q})$ is determined by minimizing $J_{\boldsymbol{q}}^-$. For $J_2/J_1 < 1/8$, a single minimum is realized at the Γ point, and for $J_2/J_1 > 1/8$, the minima are extensively degenerate and realized on the "spiral surface."

The triplon gap is closed at a critical SOC that coincides with the Weiss mean-field result. For $J_2/J_1 > 1/8$, the enhanced density of states at low energies at the criticality implies a specific heat behavior $C_v \propto T$ at low temperatures [24,27]. This behavior should be modified at the zero-temperature limit since the accidental continuous degeneracy in the momentum space would be lifted by fluctuations. On the other hand, for $J_2/J_1 < 1/8$, there is only a single critical mode at the criticality; hence, one expects a conventional $C_v \propto T^3$ behavior up to a logarithmic correction from fluctuations beyond the mean-field theory.

IV. RESPONSE TO MAGNETIC FIELD

The response to external magnetic field provides an important and visible characterization of the phase transition from the spin-orbital singlet to the ordered phase. It is of experimental interest to understand whether the magnetic field enhances the magnetic order like the case for dimerized magnets [28] or suppresses the magnetic order like the case

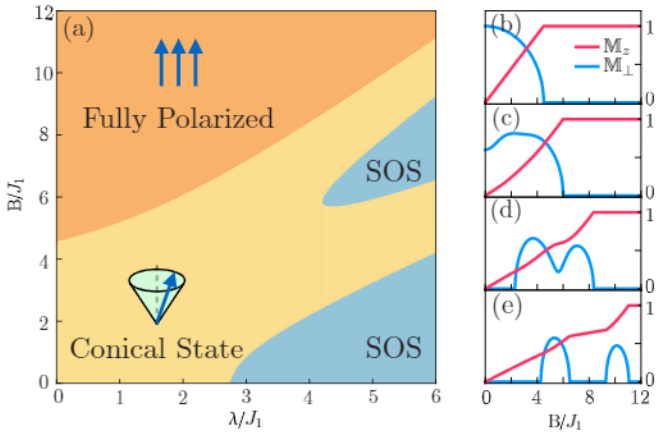

FIG. 3. (a) The phase diagram under external magnetic fields. We have fixed $J_2/J_1 = 1/4$ in the plot. Here, "SOS" refers to the spin-orbital singlet. There is a region that supports reentrant transitions between the conical state and the spin-orbital singlet state as the field is varied. (b)–(e) The magnetization curves for $\lambda/J_1 = 0, 2, 4, 6$, respectively.

for $FeSc_2S_4$ [3,4,6,7]. We consider the Zeeman coupling,

$$H_{\text{Zeeman}} = -\sum_i B\left(L_i^z + 2S_i^z\right). \tag{16}$$

Including the Zeeman coupling, our mean-field Hamiltonian now becomes $H'_{\text{MFT}} = H_{\text{MFT}} + H_{\text{Zeeman}}$.

With the magnetic field, the mean-field ansatz is adapted as

$$\boldsymbol{r}_j \in \text{I}, \quad \langle \boldsymbol{S}_j \rangle = \mathbb{M}_\perp \text{Re}[(\hat{x} - i\hat{y})e^{i\boldsymbol{q}\cdot\boldsymbol{r}_j}] + \mathbb{M}_z\hat{z}, \tag{17}$$

$$\boldsymbol{r}_j \in \text{II}, \quad \langle \boldsymbol{S}_j \rangle = \mathbb{M}_\perp \text{Re}[(\hat{x} - i\hat{y})e^{i(\boldsymbol{q}\cdot\boldsymbol{r}_j + \phi_{\boldsymbol{q}})}] + \mathbb{M}_z\hat{z}, \tag{18}$$

where $\mathbb{M}_\perp$ and $\mathbb{M}_z$ are determined self-consistently from the mean-field Hamiltonian H'_{MFT} and represent the magnetizations on the xy plane and along the z axis, respectively.

In Fig. 3, we depict the phase diagram of H'_{MFT} for a fixed J_2/J_1. The response to external magnetic field varies for different strengths of the SOC and, more precisely, differs significantly for the initial state of the system at the zero field and thus provides a characterization of the ground state. In the limit $\lambda \to 0$, H'_{MFT} reduces to $H_{\text{ex}} + H_{\text{Zeeman}}$. From the initial spiral order, our mean-field theory yields $\mathbb{M}_\perp = [1 - (B/\tilde{J})^2]^{\frac{1}{2}}$ and $\mathbb{M}_z = B/\tilde{J}$ when $B < \tilde{J}$, where $\tilde{J} \equiv 4J_1$ for $J_2/J_1 < 1/8$ and $\tilde{J} \equiv J_1^2/(8J_2) + 8J_2 + 2J_1$ for $J_2/J_1 > 1/8$. The system is fully polarized when $B > \tilde{J}$ [see Figs. 3(a) and 3(b)].

Switching on SOC but keeping λ lower than the critical value at the zero field such that the ground state has the spiral order, we find that the magnetization curve differs from the limit with $\lambda \to 0$. A small magnetic field brings down one of the $J = 1$ triplet states and thus enhances the spiral magnetization component $\mathbb{M}_\perp$ that would be suppressed by SOC and at same time brings a linear growth of the out-of-plane magnetization $\mathbb{M}_z$. As the field is further increased, the system enters a fully polarized state [see Fig. 3(c)], and $\mathbb{M}_\perp$ is then suppressed. This explains the left part of the phase diagram in Fig. 3(a), where the coexisting region of $\mathbb{M}_\perp$ and $\mathbb{M}_z$ is dubbed the "conical state."

When the strength of SOC is greater than the critical value, the mean-field ground state at the zero field is a spin-orbital singlet. The polarized moment $\mathbb{M}_z$ still grows linearly as the magnetic field is switched on, while a nonzero $\mathbb{M}_\perp$ emerges only at a critical field and shows a double-dome structure [see Fig. 3(d)]. For an even stronger SOC, the $M_\perp$ curve evolves into two separated domes, as shown in Fig. 3(e). This is what happens in the right part of the phase diagram in Fig. 3(a), where the system shows reentrant transitions between the spin-orbital singlet and the conical state before being fully polarized when the field is very strong.

The peculiar double-dome structure of the magnetization and the reentrant transitions under the magnetic field are intimately connected to the spin-orbit-entangled structure of the local moments. Let us consider the strong SOC limit where the single-ion ground state of the local moment is a spin-orbital singlet with a total moment $J = 0$. Due to different g factors for the orbital angular momentum and spin, H_{Zeeman} conserves J^z while mixing states with different J. This gives the direct consequence that the $J^z = 0$ singlet state can gain energy from the growth of $\mathbb{M}_z$ when the magnetic field is switched on [6]. As the magnetic field increases, it brings down a $J^z = 1$ state from the triplets and a $J^z = 2$ state from the higher quintuplets successively. Thus, the single-ion ground-state level crossing happens twice, and the crossing points expand to finite ranges due to the bandwidth brought by the exchange interaction, corresponding to the double-dome structure in the $\mathbb{M}_\perp$ curve, where the domes fuse together for large enough exchange interaction. This explains the structure of the magnetic phase diagram in Fig. 3(a).

It is illuminating to compare our results to that for dimerized magnets, where the field-driven Bose-Einstein condensation of triplons (and quintuplons) from the dimerized ground state happens following the same argument as above [28], leading to a similar single- (double-) dome structure in the $\mathbb{M}_\perp$ curve for spin-1/2 (spin-1) dimerized magnets. On the other hand, $\mathbb{M}_z$ there grows only within the domes in the $\mathbb{M}_\perp$ curve and becomes a plateau out of that [28–31], which differs from the results here. The field response of our model is also quite different from that of $FeSc_2S_4$, where the magnetic order will be suppressed under the field [3,4]. All three cases can be naturally understood from the evolution of the single-ion level scheme under the magnetic field that is summarized in Appendix B. From our simple comparison, we immediately conclude that the double-dome structure in the magnetization curve and the reentrant transitions here reflect the entangled structure of the spin and the orbitals in H_{soc}.

V. UNIAXIAL STRAIN

We introduce the perturbation from the uniaxial strain that is modeled by

$$H_{\text{Uni}} = -U\sum_i \left(L_i^z\right)^2. \tag{19}$$

This term is designed to capture the tetragonal distortion that often occurs in the spinel families. Another common distortion is trigonal distortion, which can be modeled differently. In its form, the tetrahedral distortion preserves the twofold degeneracy of the xz and yz orbitals [24]. Apparently,

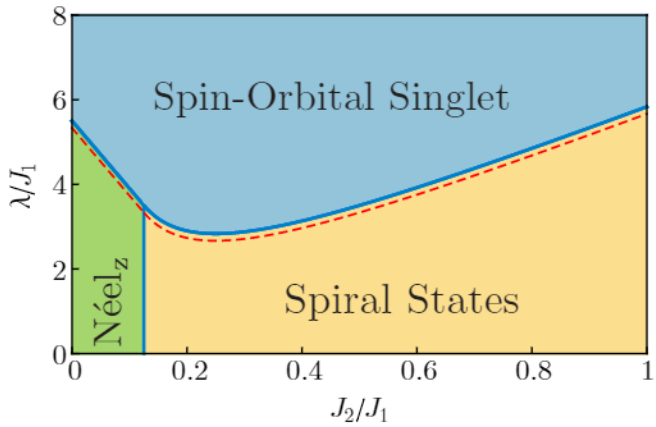

FIG. 4. The phase diagram with uniaxial strain $U/J_1 = 0.5$. The Néel$_z$ phase indicates that the Néel order is along the z axis. For comparison, the red dashed line gives the original boundary between the spin-orbital singlet and the magnetic ordered phases when $U/J_1 = 0$.

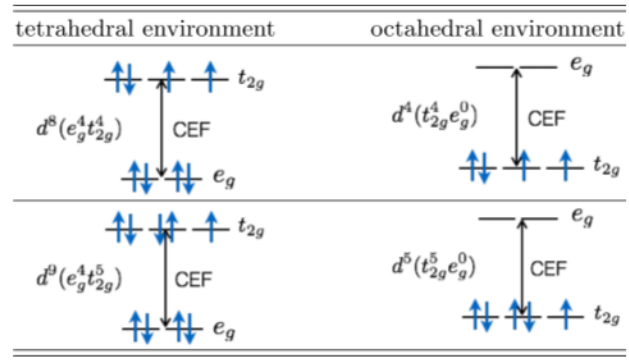

FIG. 5. The correspondence between different electron configurations in the tetrahedral and octahedral environments. The second row indicates the possibility of exploring physics similar to iridates and Kitaev physics [1,37] in d^9 materials [38].

the diamond lattice antiferromagnet $NiRh_2O_4$ experiences a tetragonal distortion at low temperatures [16,32]. A recent study explored the combination of the tetragonal distortion and the SOC and considered a stronger tetragonal distortion [33].

To explore the effect of the uniaxial strain, we start again from the spin-orbital singlet and study its excitations and instability using the flavor-wave approach introduced in Sec. III. With the uniaxial strain term $H_{\rm Uni}$, the flavor-wave mean-field Hamiltonian becomes

$$H'_{\rm fMF} = H_{\rm fMF} + \sum_{i\alpha} \frac{U}{6} t^\dagger_{i\alpha} t_{i\alpha} - \sum_i \frac{U}{2} t^\dagger_{iz} t_{iz}. \tag{20}$$

The uniaxial strain lowers the energy of the $t_{i,z}$ mode and splits the threefold degeneracy, as expected. The dispersion of the triplon excitation now reads

$$\omega_z^{\pm}(\boldsymbol{q}) = (\lambda - U/3)^{\frac{1}{2}}(\lambda - U/3 + 4J_{\boldsymbol{q}}^{\pm}/3)^{\frac{1}{2}}, \tag{21}$$

$$\omega_{xy}^{\pm}(\boldsymbol{q}) = (\lambda + U/6)^{\frac{1}{2}}(\lambda + U/6 + 4J_{\boldsymbol{q}}^{\pm}/3)^{\frac{1}{2}}, \tag{22}$$

where $\omega_z^{\pm}(\boldsymbol{q})$ are not degenerate and $\omega_{xy}^{\pm}(\boldsymbol{q})$ are twofold degenerate.

The triplon gap is closed at a critical SOC whose strength is raised by $U/3$ compared to the one without the uniaxial strain; that is, the magnetic order is enhanced (see Fig. 4). For $J_2/J_1 < 1/8$, Néel order along the z axis is stabilized from condensing $\omega_z^-(\boldsymbol{q})$ at the Γ point. For $J_2/J_1 > 1/8$, the minima of $\omega_z^-(\boldsymbol{q})$ are realized on the "spiral surface," and generally, the critical modes prefer a magnetic order with nonuniform magnitude on each site. We dub this ordered region the "spiral state" in Fig. 4.

VI. DISCUSSION

In summary, we proposed a simple spin-orbital model for a diamond lattice antiferromagnet that was inspired by the compound $NiRh_2O_4$ and related systems, capturing the competition between the atomic SOC and the exchange interaction. We point out that this competition in our model could lead to a quantum criticality between the spin-orbital singlet and the magnetic ordered states. We further study the unique response behavior of our model to the magnetic field and the perturbation effect from the uniaxial strain.

The material $NiRh_2O_4$ shows an $R\ln 6$ magnetic entropy that is greater than the pure spin-1 moments [16], indicating the presence of additional (twofold) orbital degrees of freedom. It is likely that this entropy arises from the residual degeneracy of the xz and yz orbitals in the presence of the tetragonal distortion [24]. Since this is the orbital degeneracy in the t_{2g} manifold, the atomic SOC is active at the linear order. The tetragonal distortion was then included on top of the SOC and the exchange interactions. We expect that our model may qualitatively describe the properties of the material and that the general physics revealed by this model could be relevant to other similar materials.

Due to the absence of obvious magnetic orders, the system is probably located on the spin-orbital singlet side. Various experimental probes could be useful to reveal the effects of spin-orbital entanglement and could probably drive the system from the spin-orbital singlet side towards the quantum criticality via pressure. To test the possible relevance of the theory to the compound, one may detect the magnetic excitations in the spin-orbital singlet and possibly the critical dynamics in the critical region through the spectroscopic and thermodynamic measurements. For example, one could use inelastic neutron scattering to detect the magnetic field dependence of the excitations, as it was performed for the powder sample of $FeSc_2S_4$ [6]. A completely opposite tendency, however, is expected for our model, as we discussed in Sec. IV. The Higgs mode (or amplitude mode) is one of the characteristic properties associated with the criticality in our model and may be probed by inelastic neutron scattering near the criticality but on the ordered side. This was previously studied in the dimerized magnet $TlCuCl_3$ [34,35] and the quasi-two-dimensional antiferromagnet Ca_2RuO_4 [36].

The atomic SOC acts quite similarly for the $3d^8$ ion in the tetrahedral environment and the $4d^4/5d^4$ electron configuration in the octahedral environment. From this observation, we list the correspondence between the electron configurations under these two crystal field environments in Fig. 5. This list can be further expanded with more examples. This

correspondence immediately suggests some of the physics on one side may be extended to the other side. For instance, doping-induced ferromagnetism and unconventional superconductivity were proposed for doped d^4 systems such as Ca_2RuO_4 [18,39]. Without much creativity, one may think such phenomena could be relevant for doped d^8 materials with tetrahedral crystal field environments.

ACKNOWLEDGMENTS

We thank J. Chamorro, T. McQueen, M. Mourigal, and O. Tchernyshyov for discussions. This work is supported by the Ministry of Science and Technology of China with Grants No. 2016YFA0301001, No. 2016YFA0300501, and No. 2018YFE0103200 and by Grant funding from Hong Kong's Research Grants Council (GRF No. 17303819).

APPENDIX A: DETAILS ON THE FLAVOR-WAVE APPROACH

In this part we describe the flavor-wave approach to the diamond lattice system,

$$H = \sum_{\langle ij\rangle} J_1 \boldsymbol{S}_i \cdot \boldsymbol{S}_j + \sum_{\langle\langle ij\rangle\rangle} J_2 \boldsymbol{S}_i \cdot \boldsymbol{S}_j + \lambda \sum_i \boldsymbol{L}_i \cdot \boldsymbol{S}_i, \tag{A1}$$

with $S = 1$ and $L = 1$. In this approach, one starts from the spin-orbital singlet side, i.e., the large-λ limit, and studies its excitations and instability. Considering the low-energy space on each site consisting of the $J = 0$ singlet and the $J = 1$ triplets and projecting out the $J = 2$ quintuplets, we introduce four flavors of bosons, $s_i, t_{ix}, t_{iy}, t_{iz}$, on each site i that are defined as

$$s_i^\dagger|0\rangle \equiv |0,0\rangle_i, \tag{A2}$$

$$t_{ix}^\dagger|0\rangle \equiv \frac{i}{\sqrt{2}}(|1,1\rangle_i - |1,-1\rangle_i), \tag{A3}$$

$$t_{iy}^\dagger|0\rangle \equiv \frac{1}{\sqrt{2}}(|1,1\rangle_i + |1,-1\rangle_i), \tag{A4}$$

$$t_{iz}^\dagger|0\rangle \equiv -i|1,0\rangle_i, \tag{A5}$$

where the states are labeled $|J, J^z\rangle$ and $|0\rangle$ is the vacuum state. A local Hilbert space constraint $s_i^\dagger s_i + \sum_\alpha t_{i\alpha}^\dagger t_{i\alpha} = 1$ is imposed, with $\alpha = x, y, z$. The original spin and orbital operators are then represented as

$$S_i^x = \Psi_i^\dagger \begin{pmatrix} 0 & -i\sqrt{\frac{2}{3}} & 0 & 0 \\ i\sqrt{\frac{2}{3}} & 0 & 0 & 0 \\ 0 & 0 & 0 & -\frac{i}{2} \\ 0 & 0 & \frac{i}{2} & 0 \end{pmatrix} \Psi_i, \tag{A6}$$

$$S_i^y = \Psi_i^\dagger \begin{pmatrix} 0 & 0 & -i\sqrt{\frac{2}{3}} & 0 \\ 0 & 0 & 0 & \frac{i}{2} \\ i\sqrt{\frac{2}{3}} & 0 & 0 & 0 \\ 0 & -\frac{i}{2} & 0 & 0 \end{pmatrix} \Psi_i, \tag{A7}$$

$$S_i^z = \Psi_i^\dagger \begin{pmatrix} 0 & 0 & 0 & -i\sqrt{\frac{2}{3}} \\ 0 & 0 & -\frac{i}{2} & 0 \\ 0 & \frac{i}{2} & 0 & 0 \\ i\sqrt{\frac{2}{3}} & 0 & 0 & 0 \end{pmatrix} \Psi_i, \tag{A8}$$

and

$$\boldsymbol{L}_i \cdot \boldsymbol{S}_i = \Psi_i^\dagger \begin{pmatrix} -2 & 0 & 0 & 0 \\ 0 & -1 & 0 & 0 \\ 0 & 0 & -1 & 0 \\ 0 & 0 & 0 & -1 \end{pmatrix} \Psi_i, \tag{A9}$$

$$\left(L_i^z\right)^2 = \Psi_i^\dagger \begin{pmatrix} \frac{2}{3} & 0 & 0 & 0 \\ 0 & \frac{1}{2} & 0 & 0 \\ 0 & 0 & \frac{1}{2} & 0 \\ 0 & 0 & 0 & 1 \end{pmatrix} \Psi_i, \tag{A10}$$

with $\Psi_i = (s_i, t_{ix}, t_{iy}, t_{iz})^T$.

In the spin-orbital singlet phase, the singlet boson s_i is condensed, with $\langle s_i\rangle \equiv s \neq 0$, and one can further require

$$s \to \left[1 - \frac{1}{N}\sum_{i\alpha} t_{i\alpha}^\dagger t_{i\alpha}\right]^{\frac{1}{2}} \approx 1 - \frac{1}{2N}\sum_{i\alpha} t_{i\alpha}^\dagger t_{i\alpha}, \tag{A11}$$

which takes the local Hilbert space constraint into account. Here, N is the number of sites.

With the above reformulation of the spin variables, we keep terms up to the second order and obtain a flavor-wave mean-field Hamiltonian for the triplet excitations,

$$H_{\mathrm{fMF}} = \sum_{\langle ij\rangle,\alpha} \frac{2J_1}{3}(t_{i\alpha}^\dagger t_{j\alpha} + t_{i\alpha}^\dagger t_{j\alpha}^\dagger + \mathrm{H.c.}) + \sum_{\langle\langle ij\rangle\rangle,\alpha} \frac{2J_2}{3}(t_{i\alpha}^\dagger t_{j\alpha} + t_{i\alpha}^\dagger t_{j\alpha}^\dagger + \mathrm{H.c.}) + \lambda \sum_{i\alpha} t_{i\alpha}^\dagger t_{i\alpha}. \tag{A12}$$

The triplon excitation can be readily found as

$$\omega^\pm(\boldsymbol{q}) = \lambda^{\frac{1}{2}}(\lambda + 4J_{\boldsymbol{q}}^\pm/3)^{\frac{1}{2}}, \tag{A13}$$

where $J_{\boldsymbol{q}}^\pm \equiv J_2 \sum_{\boldsymbol{b}_i} e^{i\boldsymbol{q}\cdot\boldsymbol{b}_i} \pm J_1 |\sum_{\boldsymbol{a}_i} e^{i\boldsymbol{q}\cdot\boldsymbol{a}_i}|$ and $\{\boldsymbol{a}_i\}$ ($\{\boldsymbol{b}_i\}$) refer to the first- (second-) neighbor vectors. Both $\omega^\pm(\boldsymbol{q})$ are threefold degenerate, and the minimum of $\omega^-(\boldsymbol{q})$ is determined by minimizing $J_{\boldsymbol{q}}^-$. For $J_2/J_1 < 1/8$, a single minimum is realized at the Γ point, and for $J_2/J_1 > 1/8$, the minima are extensively degenerate and realized on the spiral surface.

For the diamond lattice, the first-neighbor vectors $\{\boldsymbol{a}_i\}$ are $\{\frac{1}{4}[111], \frac{1}{4}[1\bar{1}\bar{1}], \frac{1}{4}[\bar{1}1\bar{1}], \frac{1}{4}[\bar{1}\bar{1}1]\}$, and three fcc lattice vectors are $\frac{1}{2}[011]$, $\frac{1}{2}[101]$ and $\frac{1}{2}[110]$; then,

$$J_{\boldsymbol{q}}^\pm = 4J_2\Lambda(\boldsymbol{q}) \pm 2J_1\sqrt{\Lambda(\boldsymbol{q}) + 1}, \tag{A14}$$

with

$$\Lambda(\boldsymbol{q}) = \cos\left(\frac{q_x}{2}\right)\cos\left(\frac{q_y}{2}\right) + \cos\left(\frac{q_x}{2}\right)\cos\left(\frac{q_z}{2}\right) + \cos\left(\frac{q_y}{2}\right)\cos\left(\frac{q_z}{2}\right). \tag{A15}$$

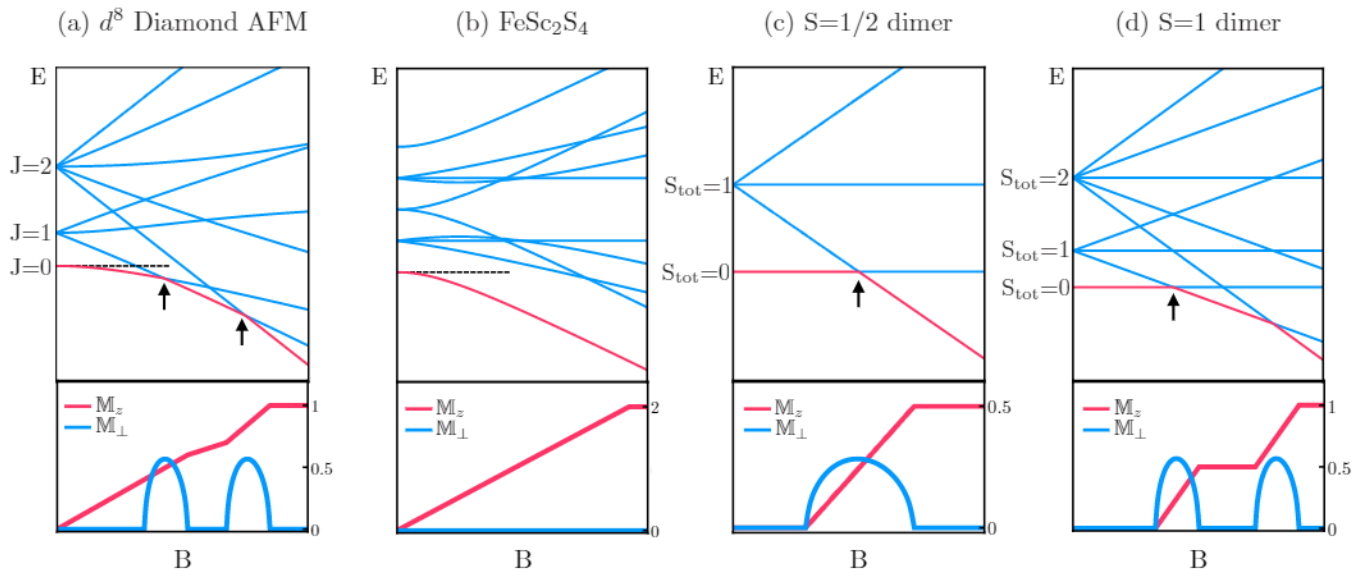

FIG. 6. Single-ion energy level schemes (top panels) and schematic magnetization curves (bottom panels) for (a) the $3d^8$ diamond lattice antiferromagnet, (b) the $S = 1$ diamond lattice antiferromagnet $FeSc_2S_4$, (c) spin-1/2 dimerized magnets, and (d) spin-1 dimerized magnets [29]. See discussion in the text.

The spiral surface is given by

$$\Lambda(q) = \frac{J_1^2}{16J_2^2} - 1. \tag{A16}$$

APPENDIX B: COMPARISON OF THE RESPONSE BEHAVIOR TO MAGNETIC FIELD OF DIFFERENT SYSTEMS

In this Appendix, we discuss the response behavior to magnetic field of (1) our model for the diamond lattice antiferromagnet, (2) the spin $S = 2$ diamond lattice antiferromagnet $FeSc_2S_4$, and (3) spin-1/2 and spin-1 dimerized magnets.

For each system, the Hamiltonian can be separated into the single-ion part H_0 and the exchange part H_{ex} (for dimerized magnets [34], the building block is the spin dimer with two spin-1/2 or spin-1 moments, H_0 is the isolated dimer part, and H_{ex} should be understood as interdimer exchange interactions). Whether the initial state of the system at the zero field is a nonmagnetic state or a magnetic ordered state depends on the strength of H_{ex}. When H_{ex} is small, in all three cases the system starts from the nonmagnetic singlet side and finally becomes fully polarized. The response behavior is directly related to the single-ion energy level scheme evolution under the magnetic field, as we show in Fig. 6.

As in the main text, we assume that the magnetic field is applied along the $\hat{z}$ direction, and $\langle S_i \rangle = \mathbb{M}_\perp \hat{n}_i + \mathbb{M}_z \hat{z}$, where $\hat{n}_i$ is a unit vector on the xy plane. So $\mathbb{M}_\perp$ and $\mathbb{M}_z$ represent the magnetizations on the xy plane and along the z axis, respectively.

The single-ion Hamiltonian of our model for the diamond lattice antiferromagnet with $3d^8$ magnetic ion reads

$$H_0 = \lambda \sum_i \boldsymbol{L}_i \cdot \boldsymbol{S}_i - \sum_i B\left(L_i^z + 2S_i^z\right)$$
$$= \lambda \sum_i (\boldsymbol{J}_i)^2/2 - \sum_i B\left(J_i^z + S_i^z\right), \tag{B1}$$

with $\lambda > 0$, spin $S = 1$, effective orbital angular momentum $L = 1$, and $\boldsymbol{J}_i \equiv \boldsymbol{L}_i + \boldsymbol{S}_i$. At the zero field, the SOC term splits the single-ion energy levels to the lowest $J = 0$ singlet, higher $J = 1$ triplets, and $J = 2$ quintuplets. Since J^z is conserved and J is not, the singlet evolves to a $\langle J \rangle \neq 0$ state and gains energy from the growth of $\mathbb{M}_z$, when the magnetic field is switched on. As the magnetic field increases, it brings down a $J^z = 1$ state from the triplets and a $J^z = 2$ state from the quintuplets successively, and the ground-state level crossing happens twice. For small but nonzero H_{ex}, the crossing points expand to finite ranges due to the bandwidth brought by the exchange interaction, leading to the double-dome structure in the $\mathbb{M}_\perp$ curve [see Fig. 6(a)]. For stronger H_{ex}, two domes will fuse together.

The single-ion Hamiltonian of $FeSc_2S_4$ can be modeled as [3]

$$H_0 = -\frac{\lambda}{3} \sum_i \left\{\sqrt{3} T_i^x \left[\left(S_i^x\right)^2 - \left(S_i^y\right)^2\right] + T_i^z \left[3\left(S_i^z\right)^2 - S_i^2\right]\right\} - \sum_i B S_i^z, \tag{B2}$$

with $\lambda > 0$, spin $S = 2$, and pseudospin $T = 1/2$, where T acts on the x^2-y^2 and $3z^2$-r^2 orbitals in the e_g subspace. The orbital angular momentum is quenched, and the magnetic field couples only to spin. Again, the lowest singlet state at zero field can gain energy from the polarization when the magnetic field is switched on. Moreover, it adiabatically evolves to the fully polarized state without level crossing, so $M_\perp$ remains zero [see Fig. 6(b)]. For strong enough H_{ex}, the initial state of the system is a magnetic ordered state with nonzero $\mathbb{M}_\perp$. The magnetic field is to suppress the magnetic order [3], leading to a monotonic decrease of $\mathbb{M}_\perp$.

For dimerized magnets, one has

$$H_0 = J_0 \sum_i S_{i,1} \cdot S_{i,2} - \sum_i B\left(S^z_{i,1} + S^z_{i,2}\right)$$
$$= J_0 \sum_i (S_{i,\mathrm{tot}})^2/2 - \sum_i B S^z_{i,\mathrm{tot}}, \quad \text{(B3)}$$

with $J_0 > 0$. Here, $S_{i,1}$ and $S_{i,2}$ are two spins on the dimer i. At zero field, J_0 splits the single-ion energy levels to the lowest $S_{\mathrm{tot}} = 0$ singlet and higher high-spin multiplets. For $S = 1/2$ dimerized magnets, the field could drive a Bose-Einstein condensation of triplons from the dimerized ground state, and the transition occurs at the point where the energy gap of the triplon is closed. Due to the local moment structure of the dimer with only singlet and triplets, there is only one dome in the $\mathbb{M}_\perp$ curve, and the ground-state level crossing happens only once. For $S = 1$ dimerized magnets, one could expect a double-dome structure in the $\mathbb{M}_\perp$ curve due to the existence of higher quintuplets, following the same argument as that for the $3d^8$ diamond lattice antiferromagnet. For both the $S = 1/2$ and $S = 1$ cases, since the magnetic field couples to only the spins, the Zeeman term conserves both S^z_{tot} and S_{tot} on each dimer. This implies that $\mathbb{M}_z$ can grow only within the ranges corresponding to level crossings, i.e., within the domes in the $\mathbb{M}_\perp$ curve, and becomes a plateau out of that [26,29]. Please refer to Fig. 6(c) [Fig. 6(d)] for the spin-1/2 (spin-1) case.

[1] W. Witczak-Krempa, G. Chen, Y. B. Kim, and L. Balents, Correlated quantum phenomena in the strong spin-orbit regime, Annu. Rev. Condens. Matter Phys. **5**, 57 (2014).

[2] G. Khaliullin, S. Maekawa, S. E. Barnes, S. Ishihara, T. Tohyama, and W. Koshibae, *Physics of Transition Metal Oxides* (Springer, Berlin, 2004).

[3] G. Chen, A. P. Schnyder, and L. Balents, Excitation spectrum and magnetic field effects in a quantum critical spin-orbital system: The case of $FeSc_2S_4$, Phys. Rev. B **80**, 224409 (2009).

[4] G. Chen, L. Balents, and A. P. Schnyder, Spin-Orbital Singlet and Quantum Critical Point on the Diamond Lattice: $FeSc_2S_4$, Phys. Rev. Lett. **102**, 096406 (2009).

[5] V. Fritsch, J. Hemberger, N. Büttgen, E.-W. Scheidt, H.-A. Krug von Nidda, A. Loidl, and V. Tsurkan, Spin and Orbital Frustration in $MnSc_2S_4$ and $FeSc_2S_4$, Phys. Rev. Lett. **92**, 116401 (2004).

[6] A. Biffin, C. Rüegg, J. Embs, T. Guidi, D. Cheptiakov, A. Loidl, V. Tsurkan, and R. Coldea, Magnetic Field Dependence of Excitations near Spin-Orbital Quantum Criticality, Phys. Rev. Lett. **118**, 067205 (2017).

[7] K. W. Plumb, J. R. Morey, J. A. Rodriguez-Rivera, H. Wu, A. A. Podlesnyak, T. M. McQueen, and C. L. Broholm, Antiferromagnetic and Orbital Ordering on a Diamond Lattice near Quantum Criticality, Phys. Rev. X **6**, 041055 (2016).

[8] C. Setty, Z. Leong, S. Zhang, and P. W. Phillips, Absence of nematic ordering transition in a diamond lattice: Application to $FeSc_2S_4$, Phys. Rev. B **95**, 020403(R) (2017).

[9] A. Krimmel, M. Mücksch, V. Tsurkan, M. M. Koza, H. Mutka, and A. Loidl, Vibronic and Magnetic Excitations in the Spin-Orbital Liquid State of $FeSc_2S_4$, Phys. Rev. Lett. **94**, 237402 (2005).

[10] L. Mittelstädt, M. Schmidt, Z. Wang, F. Mayr, V. Tsurkan, P. Lunkenheimer, D. Ish, L. Balents, J. Deisenhofer, and A. Loidl, Spin-orbiton and quantum criticality in $FeSc_2S_4$, Phys. Rev. B **91**, 125112 (2015).

[11] S. Sarkar, T. Maitra, R. Valentí, and T. Saha-Dasgupta, Comparative study of $FeCr_2S_4$ and $FeSc_2S_4$: Spinels with orbitally active *A* site, Phys. Rev. B **82**, 041105(R) (2010).

[12] N. J. Laurita, J. Deisenhofer, L. Pan, C. M. Morris, M. Schmidt, M. Johnsson, V. Tsurkan, A. Loidl, and N. P. Armitage, Singlet-Triplet Excitations and Long-Range Entanglement in the Spin-Orbital Liquid Candidate $FeSc_2S_4$, Phys. Rev. Lett. **114**, 207201 (2015).

[13] G. Jackeli and G. Khaliullin, Magnetically Hidden Order of Kramers Doublets in d^1 Systems: Sr_2VO_4, Phys. Rev. Lett. **103**, 067205 (2009).

[14] K. Matsuura, H. Sagayama, A. Uehara, Y. Nii, R. Kajimoto, K. Kamazawa, K. Ikeuchi, S. Ji, N. Abe, and T. Arima, Spin-Orbital Correlated Dynamics in the Spinel-Type Vanadium Oxide MnV_2O_4, Phys. Rev. Lett. **119**, 017201 (2017).

[15] L. D. Tung, A. Ivanov, J. Schefer, M. R. Lees, G. Balakrishnan, and D. McK. Paul, Spin, orbital ordering, and magnetic dynamics of $LaVO_3$: Magnetization, heat capacity, and neutron scattering studies, Phys. Rev. B **78**, 054416 (2008).

[16] J. R. Chamorro, L. Ge, J. Flynn, M. A. Subramanian, M. Mourigal, and T. M. McQueen, Frustrated spin one on a diamond lattice in $NiRh_2O_4$, Phys. Rev. Mater. **2**, 034404 (2018).

[17] G. Chen and L. Balents, Spin-orbit coupling in d^2 ordered double perovskites, Phys. Rev. B **84**, 094420 (2011).

[18] G. Khaliullin, Excitonic Magnetism in Van Vleck–type d^4 Mott Insulators, Phys. Rev. Lett. **111**, 197201 (2013).

[19] K. I. Kugel' and D. I. Khomski, The Jahn-Teller effect and magnetism: Transition metal compounds, Sov. Phys. Usp. **25**, 231 (1982).

[20] D. Bergman, J. Alicea, E. Gull, S. Trebst, and L. Balents, Order-by-disorder and spiral spin-liquid in frustrated diamond-lattice antiferromagnets, Nat. Phys. **3**, 487 (2007).

[21] F. L. Buessen, M. Hering, J. Reuther, and S. Trebst, Quantum Spin Liquids in Frustrated Spin-1 Diamond Antiferromagnets, Phys. Rev. Lett. **120**, 057201 (2018).

[22] S. Lee and L. Balents, Theory of the ordered phase in *A*-site antiferromagnetic spinels, Phys. Rev. B **78**, 144417 (2008).

[23] L. Savary, E. Gull, S. Trebst, J. Alicea, D. Bergman, and L. Balents, Impurity effects in highly frustrated diamond-lattice antiferromagnets, Phys. Rev. B **84**, 064438 (2011).

[24] G. Chen, Quantum paramagnet and frustrated quantum criticality in a spin-one diamond lattice antiferromagnet, Phys. Rev. B **96**, 020412(R) (2017).

[25] J.-S. Bernier, M. J. Lawler, and Y. B. Kim, Quantum Order by Disorder in Frustrated Diamond Lattice Antiferromagnets, Phys. Rev. Lett. **101**, 047201 (2008).

[26] M. Matsumoto, B. Normand, T. M. Rice, and M. Sigrist, Field- and pressure-induced magnetic quantum phase transitions in $TlCuCl_3$, Phys. Rev. B **69**, 054423 (2004).

[27] G. Chen, M. Hermele, and L. Radzihovsky, Frustrated Quantum Critical Theory of Putative Spin-Liquid Phenomenology in $6H$-B-$Ba_3NiSb_2O_9$, Phys. Rev. Lett. **109**, 016402 (2012).

[28] V. Zapf, M. Jaime, and C. D. Batista, Bose-Einstein condensation in quantum magnets, Rev. Mod. Phys. **86**, 563 (2014).

[29] E. C. Samulon, Y. Kohama, R. D. McDonald, M. C. Shapiro, K. A. Al-Hassanieh, C. D. Batista, M. Jaime, and I. R. Fisher, Asymmetric Quintuplet Condensation in the Frustrated $S = 1$ Spin Dimer Compound $Ba_3Mn_2O_8$, Phys. Rev. Lett. **103**, 047202 (2009).

[30] M. Uchida, H. Tanaka, H. Mitamura, F. Ishikawa, and T. Goto, High-field magnetization process in the $S = 1$ quantum spin system $Ba_3Mn_2O_8$, Phys. Rev. B **66**, 054429 (2002).

[31] M. Uchida, H. Tanaka, M. I. Bartashevich, and T. Goto, Singlet ground state and magnetization plateaus in $Ba_3Mn_2O_8$, J. Phys. Soc. Jpn. **70**, 1790 (2001).

[32] S. Horiuti and S. Miyahara, Tetragonal distortion of $NiRh_2O_4$, J. Phys. Soc. Jpn. **19**, 423 (1964).

[33] S. Das, N. Dhani, T. Saha-Dasgupta, and A. Paramekanti, The curious case of $NiRh_2O_4$: A spin-orbit entangled diamond lattice paramagnet, arXiv:1905.11403.

[34] P. Merchant, B. Normand, K. W. Krämer, M. Boehm, D. F. McMorrow, and C. Rüegg, Quantum and classical criticality in a dimerized quantum antiferromagnet, Nat. Phys. **10**, 373 (2014).

[35] C. Rüegg, B. Normand, M. Matsumoto, A. Furrer, D. F. McMorrow, K. W. Krämer, H. U. Güdel, S. N. Gvasaliya, H. Mutka, and M. Boehm, Quantum Magnets under Pressure: Controlling Elementary Excitations in $TlCuCl_3$, Phys. Rev. Lett. **100**, 205701 (2008).

[36] A. Jain, M. Krautloher, J. Porras, G. H. Ryu, D. P. Chen, D. L. Abernathy, J. T. Park, A. Ivanov, J. Chaloupka, G. Khaliullin, B. Keimer, and B. J. Kim, Higgs mode and its decay in a two-dimensional antiferromagnet, Nat. Phys. **13**, 633 (2017).

[37] S. Trebst, Kitaev materials, arXiv:1701.07056.

[38] L. Ge, J. Flynn, J. A. M. Paddison, M. B. Stone, S. Calder, M. A. Subramanian, A. P. Ramirez, and M. Mourigal, Spin order and dynamics in the diamond-lattice Heisenberg antiferromagnets $CuRh_2O_4$ and $CoRh_2O_4$, Phys. Rev. B **96**, 064413 (2017).

[39] J. Chaloupka and G. Khaliullin, Doping-Induced Ferromagnetism and Possible Triplet Pairing in d^4 Mott Insulators, Phys. Rev. Lett. **116**, 017203 (2016).